Semnan University

Progress in Physics of Applied Materials

journal homepage: https://ppam.semnan.ac.ir/

# The effect of different substitutions (Eu, Ce, Al, and Bi) on the structural and magnetic properties of $Fe_3O_4$

**S. Esmaeili [a*], M. Aghazadeh[b], I. karimzadeh[c], F. Shokriyan [a]**

[a] *Faculty of Physics, Semnan University, P.O. Box: 35195-363, Semnan, Iran*
[b] *Materials and Nuclear Research School, Nuclear Science and Technology Research Institute (NSTRI), P.O. Box 14395-834, Tehran, Iran*
[c] *Department of Physics, Faculty of Science, Central Tehran Branch, Islamic Azad University, Tehran, Iran*

**ARTICLE INFO**

Article history:
Received: 07 May 2022
Revised: 07 July 2022
Accepted: 14 July 2022

Keywords:
$Fe_3O_4$ ferrite
Substitutions
Cathodic electrical deposition method
Magnetic properties

**ABSTRACT**

In this study, the effect of different substitutions (Eu, Ce, Al, and Bi) on the structural and magnetic properties of $Fe_3O_4$ is investigated. All samples were synthesized with the cathodic electrochemical deposition method. The structural properties and surface morphology are investigated by XRD and FESEM analyses. Structural analysis of the samples showed the formation of a single-phase structure with an *Fd*-3*m* space group. The results also showed that the lattice constant and the cell volume increase by increasing the substituted ion's radius. The results of surface morphology of the samples also showed that with increasing substituted ion radius, the average diameter of the samples increases. For $BiFe_2O_4$, $EuFe_2O_4$, $CeFe_2O_4$, and $AlFe_2O_4$ samples, the mean diameter was obtained at 50.038 (±13.60)nm, 47.95 (±9.62)nm, 36.06 (±8.29)nm, and 45.72 (±5.39)nm, respectively. And, the magnetic properties of the samples were investigated by VSM analysis. The study of the magnetic properties of the samples shows the superparamagnetic behavior for all samples. Also, the results show that substituting Fe ions with larger radii ions leads to a decrease in saturation magnetization ($M_s$) and residual magnetization ($M_r$).

## 1. Introduction

At present, magnetic nanoparticles are considered for further research due to their many applications, such as the drugs delivery to the desired points in the body, disease diagnosis, water treatment, computer memory, and sensors [1-3]. Previous studies have shown that magnetic properties strongly depend on particle size, number of interactions, methods of preparing nanoparticles, etc. Since magnetic nanoparticles are usually agglomerated, there is a dipole-bipolar interaction among the the particles due to the proximity of all particles. This interaction can harm their application in the mentioned cases. There are different types of ferrites, including hexaferrite, garnet ferrite, ortho-ferrite, and spinel ferrite [4-6]. The other advantage of ferrites over magnetic materials such as iron and other alloys is their high strength, which allows them to perform better at high frequencies[7, 8]. Some ferrites have a spinel structure in the form of AB2O4 so that A and B represent the tetrahedral and octahedral cations, respectively, and O represents the anions. Since divalent ions are larger than trivalent ions, it makes sense for divalent ions to be in octahedral positions and trivalent ions in quadrilateral locations. Still, there is one exception that divalent ions tend to occupy quadrilateral positions [9, 10]. Common form of ferrite is $MFe_2O_4$, where M can be metals such as Zn, Fe, Mg, Co, Ni, Mn [11-14]. Spinel ferrite nanoparticles are widely studied due to their excellent and suitable magnetic and electrical properties [15, 16]. Abrasion resistance and electrical insulation are widely considered. The magnetic properties of materials depend on the nanoparticles' size, shape, and purity.

So far, many studies have been done on ferrites' structural and magnetic properties. For example, Dippong et al. [17] examined the effect of Ni substitution (0-1%) on the magnetic and structural properties of Manganese Ferrite. The results revealed that increasing the substitution leads to secondary phases in the crystalline structure. This increase also leads to a decrease in the coercivity field and shows the paramagnetic behavior structure. Tancredi et al. [18] examined the effect of substitution on magnetic and structural properties of cobalt ferrite. The results revealed that with increasing cobalt substitution, the magnetic properties of the structure are improved. In this study, the saturation magnetization (Ms) and the coercivity (Ce) increased with increasing substitution. Mulushoa et al. [19] examined the effect of Nickel-Chromium substitution on the magnetic and structural properties of Magnesium ferrites. The results revealed that the Ms and Ce increase with increasing Chromium substitution. Kumar et al. [20] examined the effect of Nd substitution on magnetic and

* Corresponding author. Tel.: +989134117161
*E-mail address:* shadi.esmaeili72@semnan.ac.ir

DOI: 10.22075/ppam.2022.27100.1029

structural properties of Co-Ni/Fe3O4 ferrite. The results revealed a single-phase structure for all samples. The results also showed that Ms and Ce increase and decrease with increasing substitution, respectively. Ahmad Gholizadeh [21] examined the effects of the preparation technique on X-ray peak broadening, magnetic and elastic moduli properties of Fe3O4 nanoparticles prepared by coprecipitation (FcP-NPs) and citrate (FC-NPs) methods. The cation distribution obtained from calculated inversion parameter indicated that in the smaller particles, more amount of $Fe^{2+}$ on the tetrahedral sites can be related to higher stress induced in the FcP-NPs compared to the FC-NPs. The saturation magnetization of the FcP-NPs was almost two times greater than the saturation magnetization of the FC-NPs. By comparison of the elastic results of FC-NPs with those of the the FcP-NPs, it was observed that the elastic properties of the F-NPs have been improved by synthesis method, while Poisson's ratio almost remains constant.

Mohamed et al. [22] examined the effect of Cu on the magnetic and structural properties of cobalt ferrites. The results revealed a spinel single cubic phase for all samples. They also showed that a significant increase in the Ms of the samples was observed with increasing copper substitution. Silva-Soares et al. [23] examined the effect of Al substitution on the magnetic properties of Ba0. 9La0. 1Fe12-xAlxO19 hexaferrite. The results revealed that with increasing aluminum up to x = 0.7, the Ms and the Ce increased to their maximum value. Crystalline magnetic anisotropy also decreased with increasing ion replacement. Previous studies show that substituting different ions significantly affects ferrites' structural and magnetic properties. From this purpose, in this study the effect of different substitutions (Eu, Ce, Al, and Bi) on the structural and magnetic properties of Fe3O4 is investigated. XRD and FESEM analyzes were performed to investigate the structural properties and surface morphology. Finally, the magnetic properties of the structure were investigated by VSM analysis.

## 2. Experimental and method

This study used the cathodic electrical deposition method to synthesize Fe3O4 nanoparticles. The chemical material used to prepare the samples in this study is 2 g of iron nitrate, 1 g of iron (II) chloride, and 0.4 g of aluminum chloride and distilled water. The precursors are placed in a steam bath at a temperature of 25 °C. An electrochemical workstation system performed this process with a current density of 10 mA/cm2. And potentiostat/galvanostat device, model: NCF-PGS 2012, Iran, was used. Deposition time was optimized to be 30 minutes. A stainless steel sheet and two graphite plates have been used in this process. The dimensions of these sheets are 5 cm ×5 cm× 0.5 mm. The steel sheet is then removed from the electrolyte and washed several times with deionized water. Finally, the deposited black film was separated from the cathode surface. A centrifuge at 6000 rpm was used for 20 minutes in this study. Finally, the sediment was separated from the aqueous solution by a magnet. The separated sediment was dried for 1 hour at 70 oC. Finally, the synthesized material was studied from a structural and magnetic point of view.

X-ray diffraction on ferrite powder samples was performed by XRD method using a PW-1800, manufactured by Philips, on a scale between 20 and 70 degrees, with a Cu-Kα1,2 source with a wavelength of 1.5418 Å. And the surface morphology of samples was examined by field emission scanning electron microscopy (FE-SEM, Mira 3-XMU with accelerating voltage of 100 kV). The magnetic properties of samples were calculated using a vibrating-sample magnetometer (VSM) (model: Meghnatis Daghigh Kavir, Iran). This device is in the range of – 20,000 to 20,000 Oe at 300 K.

## 3. Results and discussion

### *3.1. XRD*

Fig. 1 represent the XRD analysis of samples. With the help of X-pert software, the transition index of X-ray diffraction lines was performed, which is shown in Figure 1. The diffraction pattern corresponded exactly to the JCPDS card number 01-075-0449, related to $Fe_3O_4$. In these patterns, no additional peaks were observed based on impurities. The (220), (311), (400), (422), (511), and (440) planes in the diffraction patterns of these nanoparticles indicate the formation of a spinel cubic structure with an *Fd*-3*m* space group. The results show that the (311) plane has the highest intensity. Examining the X-ray diffraction patterns of the samples, it can be seen that the position of these peaks changes with different substitutions in the samples (see Figure 1 (b)).

The crystallite size ($D$) of the samples is calculated by using Scherrer equation (1) [24], where, $\lambda$ is the X-ray wavelength, and $d$ is the distance of the parallel planes with the Miller indices h, k, and l are calculated from equation (2). In equation (2), $\theta$, and $n$ are the angle and diffraction order, respectively. The calculated values are shown in Table 1.

$$D = \frac{0.98\lambda}{\beta \operatorname{Cos}\theta} \tag{1}$$

$$2d \operatorname{Sin}\theta = n\lambda \tag{2}$$

The results showed that by changing the substitution in ferrite samples, partial displacement of the peaks towards smaller angles is seen due to the increase of the lattice constant (a). This increase is due to replacing cations with larger ion radius (Eu=0.11 nm, Bi=0.10 nm, Ce= 0.10 nm, and Al= 0.05 nm) instead of iron cations (0.06 nm) [25]. It has a larger ion radius, which causes the lattice to shrink, resulting reduction in the lattice constant. Eu, Al, Ce, and Bi ions are greater in size with respect to Fe ions, generally present at grain boundaries, which restrict grain growth but induce lattice strain resulting into change in crystallite size and lattice parameter. It is clear that with the substitution of these ions in $Fe_3O_4$ the major peak shifted to a lower angle. As can be seen in Table 1, with the increase of the ionic radius, the crystallite size has increased from 6.82 nm to 11.03 nm, and also the increase in the lattice constant has occurred with the increase of the ionic radius. The bond angle and bond length have not changed much. To further investigate the structural properties of the

samples, the XRD of the samples was analyzed with Fullprof softwar.

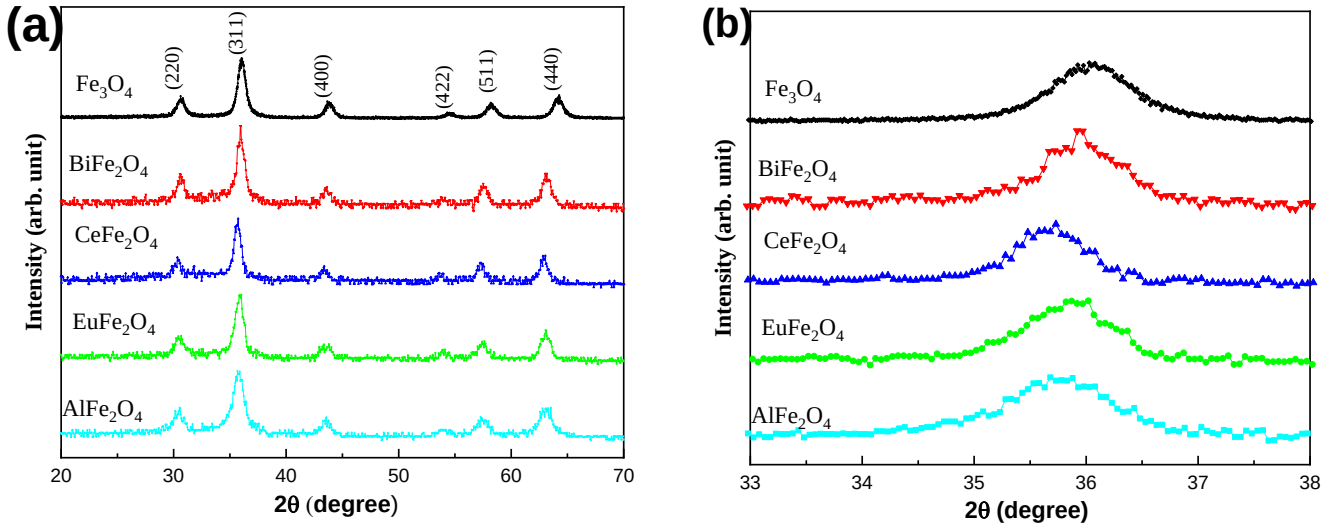


**Fig. 1.** (a) XRD pattern of samples and (b) the magnification of XRD pattern.

**Table 1.** Structural parameters of $Fe_3O_4$, $BiFe_2O_4$, $EuFe_2O_4$, $CeFe_2O_4$, and $AlFe_2O_4$.

| Samples | $Fe_3O_4$ | $BiFe_2O_4$ | $EuFe_2O_4$ | CeFe2O4 | AlFe2O4 |
|---|---|---|---|---|---|
| a (Å) | 8.30 | 8.37 | 8.35 | 8.37 | 8.30 |
| V(Å$^3$) | 582.28 | 586.7966 | 582.3922 | 586.5865 | 583.2085 |
| $\Theta_{Fe\text{-}O}$ ($^0$) | 109.47(1) | 109.47(3) | 109.47(4) | 109.47(4) | 109.47(1) |
| $d_{Fe\text{-}O}$ (Å) | 1.93 | 1.93 | 1.93 | 1.93 | 1.93 |
| $D_{Scher}$ (nm) | 7.1 | 10.5 | 11.03 | 10.5 | 6.82 |
| d (Å) | 2.49 | 2.50 | 2.51 | 2.50 | 2.49 |

### *3.2 FE-SEM analyses.*

The FE-SEM images are shown in Figure 4 (scale bar 200 nm). As shown in the figures, the particles have grown spherically. The mean particle size of the specimens shown in these image was calculated using the Digimizer software. The mean particle size of samples fits the Log-Normal function (equation 3). The mean value of the particle and its error are calculated using equations (4) and (5).

$$F(D)=\left(\frac{1}{\sigma D\sqrt{2\pi}}\right)\exp\left[-\frac{ln^2\left(\frac{D}{D_0}\right)}{2\sigma^2}\right] \quad (3)$$

$$\langle D\rangle = D_0\exp\left(\sigma^2/2\right) \quad (4)$$

$$\sigma_D=\langle D\rangle\left[exp\left(\sigma^2\right)-1\right]^{1/2} \quad (5)$$

The results show that the sample substituted with bismuth has a larger average particle diameter than other samples. Also, the particle diameter of the samples is reduced from the sample substituted with Eu, Al, and Ce, respectively. The change in the average particle diameter of the samples is related to the substitution of particles with different radii relative to each other. The estimated results are reported in Table 2. The crystallite size is smaller than the particle size, and this indicates that each particle in the image can be a single crystal.

### *3.3. VSM analysis*

Ferrites are chemical compounds with the formula $AB_2O_4$, where A and B represent different metal cations; they usually contain iron. Ferrite is a class of spinels in which divalent, trivalent, and tetravalent cations can occupy A and B cavities. Spinel ferrite unit cell contains 32 oxygen, 16 trivalent iron and 8 divalent metal ions. One of the most important features of the unit cell is that the arrangement of oxygen ions creates two types of holes, which are filled by metal ions. These holes are called tetrahedral or A and octahedral or B. Oxygen ions in the spinel structure are formed from the fcc lattice, and $A^{+2}$ and $B^{+3}$ ions occupy octahedral and tetrahedral interspaces, depending on the type of spinel. The structure of spinel is normal spinel and reverse spinel. In reverse spinels, divalent metal ions are placed in B sites and trivalent metal ions are placed equally in A and B sites. In normal spinel, non-magnetic ions occupy the A cavity and thus there is no AB interaction. The negative interaction of BB dominates and the trivalent iron ions are aligned in a non-parallel manner, resulting in net zero magnetization. To evaluate the magnetic properties, the hysteresis loops of the samples were examined. Fig. 4 represents the VSM curves of samples at room temperature in the 1,000 Oe magnetic field. In general, applying a magnetic field to a magnetic material causes the walls of the domain to move along the crystal. With the application of more fields, the structure of

several matter domains becomes a single-domain structure. Intrinsic factors (lattice defects, lattice strains,

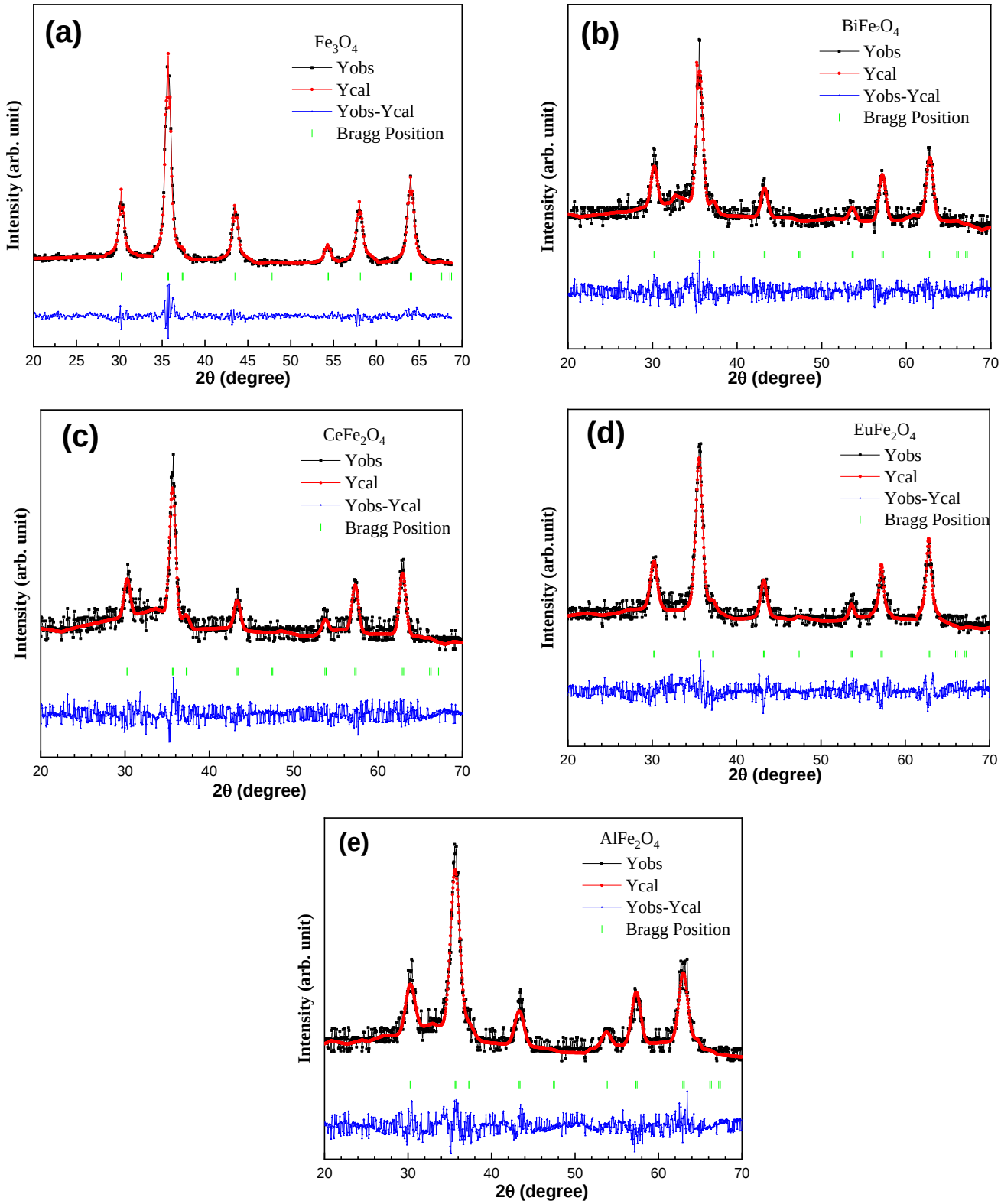


**Fig. 2.** Fullprof patterns of the samples.

**Table 2.** The mean value of the samples diameter and their error.

| Sample's diameter (nm) | $Fe_3O_4$ | $BiFe_2O_4$ | $EuFe_2O_4$ | $CeFe_2O_4$ | $AlFe_2O_4$ |
|---|---|---|---|---|---|
| $\langle D\rangle_{SEM}$ ($\pm\sigma_D$) | 40.87 (±18.31) | 50.038 (±13.60) | 47.95 (±9.62) | 36.06 (±8.29) | 45.72 (±5.39) |

and chemical impurities) play an important role in displacing basin walls. Strong fields overcome anisotropy, and the magnetism reaches a constant saturation magnetism value. The magnetic behavior of ferrites is

strongly dependent on the size of their particles. This is because, in larger nanoparticles, higher crystallization and a small amount of lattice microstructural imperfections allow the field walls to move easily in sample magnetization. On the other hand, the magnetization of spinel ferrites depends on the distribution of metal cations at both sites (A and B sites).

To calculate the $M_s$, the $C_e$, and the remaining magnetic ($M_r$), all sample curves fit with a Langevin equation (6) [26].

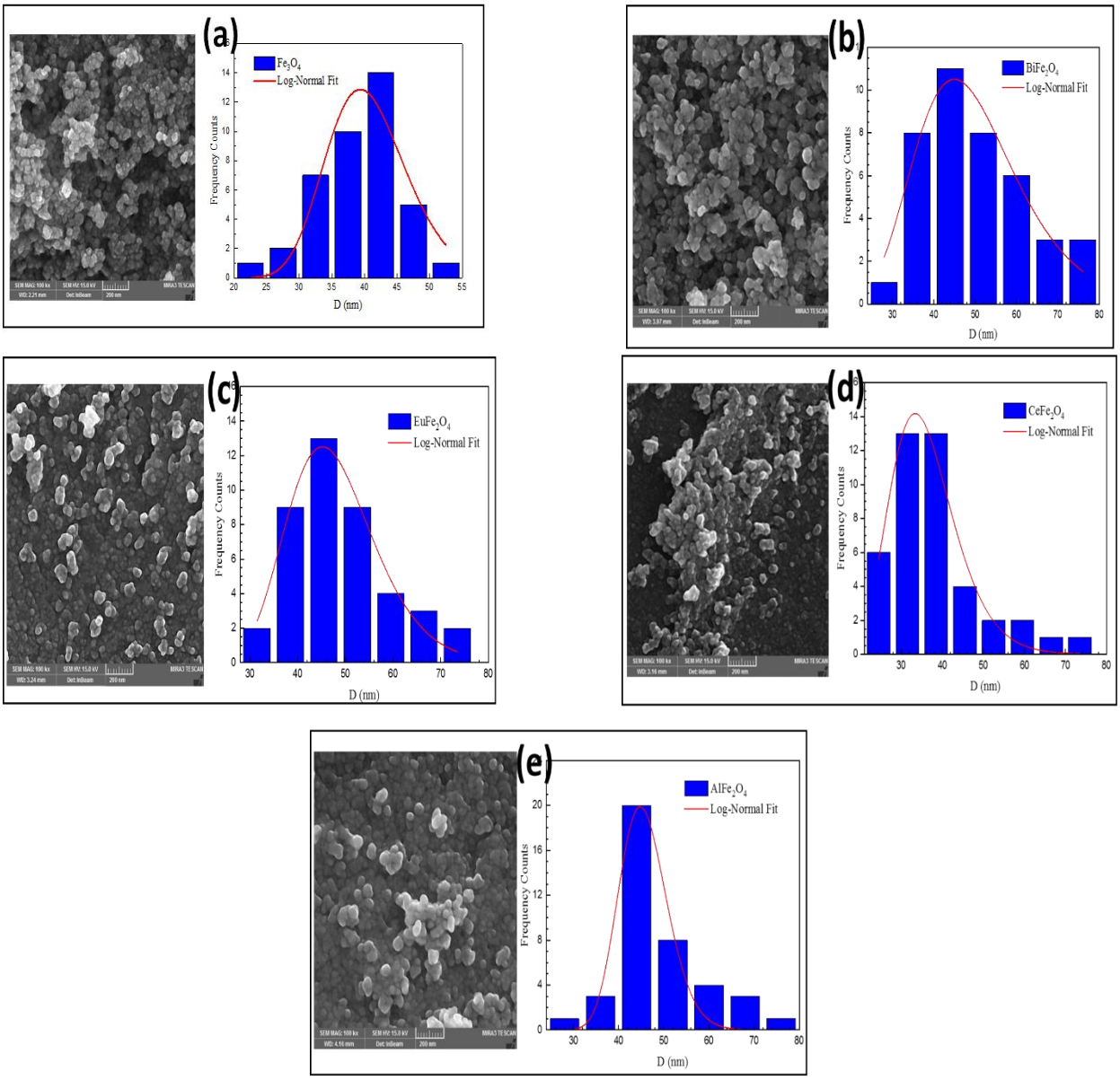


**Fig. 3.** FE-SEM images and mean diameter values of (a) $Fe_3O_4$, (b) $BiFe_2O_4$, (c) $EuFe_2O_4$, (d) $CeFe_2O_4$, and (e) $AlFe_2O_4$ samples.

$$M = M_s\, L\left(\frac{\mu_p H}{k_B T}\right) + \chi H \qquad (6)$$

here, $M$ represents the magnetism, $\mu_p$ represents the mean (super spin) moment, $H$ represents the magnetic field, $k_B$ represents the Boltzmann constant ($1.380649\times10^{-23}$ $m^2.kg.s^{-2}.K^{-1}$), and $\chi$ represents the surface spin susceptibility [26]. The study of the magnetic properties of the samples shows the behavior of the superparamagnetic behavior for all samples. The results show that the $M_s$ and $M_r$ values are reduced by changing the substitution at the iron site. This change can be attributed to inherent factors such as the preferential occupation of cubic lattice position. Among the samples, $Fe_3O_4$ has the highest $M_s$ (66.65 emu/g). By changing the substitution of Bi, Eu, Ce, and Al, the $M_s$ in the sample decreased, respectively. The oxygen vacancies and meta-cations substitution in magnetite phase destroys the

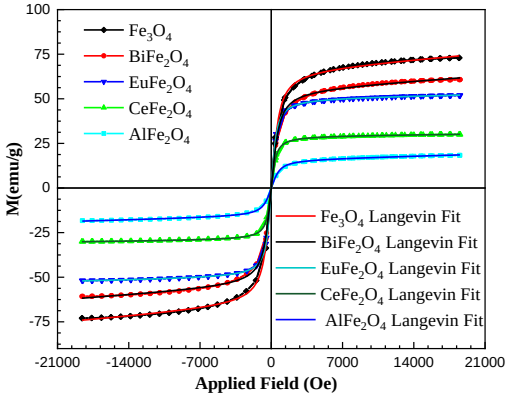

**Fig. 4.** VSM curves of samples at room temperature.

grains and lowers the saturation magnetization of the prepared ferrite powder [16]. In the case of our prepared doped $Fe_3O_4$ samples, it is observed that the saturation magnetization is lowered with different cations doping. Saturation magnetization is a function of particle size, amount of crystallinity and impurity in all samples after doping due to the introduction of crystal defects and microstrains, the residual force and saturation magnetization decreased. The results are reported in Table 3.

**Table 3.** Fitting parameters from the VSM curves

| Samples | $Fe_3O_4$ | $BiFe_2O_4$ | $EuFe_2O_4$ | $CeFe_2O_4$ | $AlFe_2O_4$ |
|---|---|---|---|---|---|
| $M_s$ (emu/g) | 66.6557 | 55.6166 | 50.6763 | 29.3323 | 16.0706 |
| $\mu_B$ | 22951.68 | 23310.3 | 33493.44 | 36506.96 | 21732.37 |
| $\chi$ | $4.6036\times10^{-4}$ | $3.786\times10^{-4}$ | $1.0538\times10^{-4}$ | $5.7929\times10^{-5}$ | $1.497\times10^{-4}$ |
| Hc (Oe) | 14.702 | 2.75 | 3.847 | 0.485 | 8.6695 |
| $M_r$ (emu/g) | 0.949 | 0.1477 | 0.2483 | 0.014 | 0.1287 |

## 4. Conclusions

In this study, the structural and magnetic properties of $Fe_3O_4$ ferrite with different substitutions (Eu, Ce, Bi, and Al) have been investigated. Samples were synthesized by the cathodic electrochemical deposition method. The results showed that all samples have a single-phase structure with an *Fd*-3*m* space group. Also, the study of the structural properties of the particles showed that with the increase of the substituted ion radii, the volume cell of samples increases. The morphology of samples is studied with FE-SEM analysis. The results of FE-SEM analysis showed that increasing the radius of the substituted ions increased the mean particle diameter. The magnetic results show that the $M_s$ and $M_r$ are reduced by changing the substitution at the iron site. The obtained results showed that $Fe_3O_4$ has the highest $M_s$ (66.65 emu/g). And by changing the substitution of Bi, Eu, Ce, and Al, the $M_s$ in the sample decreased to 55.6166, 50.6763, 29.3323, and 16.0706 emu/g, respectively.

## References


[1] N. Senthilkumar, P.K. Sharma, N. Sood, and N. Bhalla, "Designing magnetic nanoparticles for in vivo applications and understanding their fate inside human body," *Coordination Chemistry Reviews,* 445 (2021) 214082.

[2] J. Moradi, M. Ghazi, M. Ehsani, and P. Kameli, "Structural and magnetic characterization of La0. 8Sr0. 2MnO3 nanoparticles prepared via a facile microwave-assisted method," *Journal of Solid State Chemistry,* 215 (2014) 1-7.

[3] M. H. Ehsani, P. Kameli, M. E. Ghazi, and F. S. Razavi, "An investigation on magnetic interacting La0. 6Sr0. 4MnO3 nanoparticles," in *Advanced Materials Research*, 829 (2014) 712-716.

[4] S. Mahmoudi and A. Gholizadeh, "Effect of non-magnetic ions substitution on the structure and magnetic properties of Y3− xSrxFe5− xZrxO12 nanoparticles," *Journal of Magnetism and Magnetic Materials,* 456 (2018) 46-55.

[5] A. Gholizadeh, "The effects of A/B-site substitution on structural, redox and catalytic properties of lanthanum ferrite nanoparticles," *Journal of Materials Research and Technology,* 8 (2019) 457-466.

[6] J. Carvalheiras, R. M. Novais, F. Mohseni, J. S. Amaral, M. P. Seabra, J. A. Labrincha, and R. C. Pullar, "Synthesis of red mud derived M-type barium hexaferrites with tuneable coercivity," *Ceramics International,* 46 (2020) 5757-5764.

[7] J.M. Silveyra, E. Ferrara, D.L. Huber, and T.C. Monson, "Soft magnetic materials for a sustainable and electrified world," *Science,* 362 (2018) eaao0195.

[8] T. Raoufi and F. Shokrian, "Study of Landau theory and universal curve on La0. 6-xGdxSr0. 4MnO3 (x= 0-0.1) manganite," *Progress in Physics of Applied Materials,* 1 (2021) 39-43.

[9] N.K. Gill, R. Puri, "Mössbauer study of Li0. 5Fe2. 5-x CrxO4 ferrites," *Spectrochimica Acta Part A: Molecular Spectroscopy,* 41(1985) 1005-1008.

[10] M. Choupani and A. Gholizadeh, "The effect of calcination temperature on the X-ray peak broadening of t-CuFe2O4," *Progress in Physics of Applied Materials,* 1 ( 2021) 19-24.

[11] M. Aparna, A.N. Grace, P. Sathyanarayanan, and N. K. Sahu, "A comparative study on the supercapacitive behaviour of solvothermally prepared metal ferrite (MFe2O4, M= Fe, Co, Ni, Mn, Cu, Zn) nanoassemblies," *Journal of Alloys and Compounds,* 745 (2018) 385-395.

[12] X. Xie, B. Wang, Y. Wang, C. Ni, X. Sun, and W. Du, "Spinel structured MFe2O4 (M= Fe, Co, Ni, Mn, Zn) and their composites for microwave absorption: A review," *Chemical Engineering Journal,* 428 (2022) 131160.

[13] Y. Ren, L. Lin, J. Ma, J. Yang, J. Feng, and Z. Fan, "Sulfate radicals induced from peroxymonosulfate by magnetic ferrospinel MFe2O4 (M= Co, Cu, Mn, and Zn) as heterogeneous catalysts in the water," *Applied Catalysis B: Environmental,* 165 (2015) 572-578.

[14] H. Ghorbani, M. Eshraghi, A.A. Sabouri, "Magnetic properties of Co0. 9Cd0. 1Fe1. 9X0. 1O4 (X= Cr, Yb) nanoparticles prepared by hydrothermal method," *Progress in Physics of Applied Materials,* 1 (2021) 50-56.

[15] A. Miri, M. Sarani, A. Najafidoust, M. Mehrabani, F. A. Zadeh, and R. S. Varma, "Photocatalytic performance and cytotoxic activity of green-synthesized cobalt ferrite nanoparticles," *Materials Research Bulletin,* 149 (2022) 111706.

[16] M. Ehsani, S. Esmaeili, M. Aghazadeh, P. Kameli, F. S. Tehrani, and I. Karimzadeh, "An investigation on the impact of Al doping on the structural and magnetic properties of Fe3O4 nanoparticles," *Applied Physics A,* 125 (2019) 1-9.

[17] T. Dippong, E.A. Levei, I.G. Deac, I. Petean, and O. Cadar, "Dependence of Structural, Morphological and Magnetic Properties of Manganese Ferrite on Ni-Mn Substitution,"

*International Journal of Molecular Sciences,* 23 (2022) 3097.

[18] P. Tancredi, P.C. Rivas-Rojas, O. Moscoso-Londoño, D. Muraca, M. Knobel, and L. M. Socolovsky, "Size and doping effects on the improvement of the low-temperature magnetic properties of magnetically aligned cobalt ferrite nanoparticles," *Journal of Alloys and Compounds,* 894 (2022) 162432.

[19] S. Y. Mulushoa, N. Murali, P. Taddesse, A. Ramakrishna, D. Parajuli, K. M. Batoo, R. Verma, R. Kumar, Y. S. Rao, and S. Hussain, "Structural, dielectric and magnetic properties of Nickel-Chromium substituted Magnesium ferrites, Mg1–xNixFe2-xCrxO4 (0≤ x≤ 0.7)," *Inorganic Chemistry Communications,* 138 (2022) 109289.

[20] S. R. Kumar, G. V. Priya, B. Aruna, M. Raju, D. Parajuli, N. Murali, R. Verma, K. M. Batoo, R. Kumar, and P. L. Narayana, "Influence of Nd3+ substituted Co0. 5Ni0. 5Fe2O4 ferrite on structural, morphological, dc electrical resistivity and magnetic properties," *Inorganic Chemistry Communications,* 136 (2022) 109132.

[21] A. Gholizadeh, "A comparative study of physical properties in Fe3O4 nanoparticles prepared by coprecipitation and citrate methods," *Journal of the american ceramic society,* 100 (2017) 3577-3588.

[22] W. Mohamed, N. Hadia, M. Alzaid, and A. M. Abu-Dief, "Impact of Cu2+ cations substitution on structural, morphological, optical and magnetic properties of Co1-xCuxFe2O4 nanoparticles synthesized by a facile hydrothermal approach," *Solid State Sciences,* 125 (2022) 106841.

[23] P. da Silva-Soares, L. da Costa-Catique, F. Guerrero, P. Mariño-Castellanos, E. Govea-Alcaide, Y. Romaguera-Barcelay, A. Rodrigues, E. Padrón-Hernández, and R. Peña-Garcia, "Investigation of structural and magnetic properties of Al substituted Ba0. 9La0. 1Fe12-xAlxO19 hexaferrites prepared by solid-state reaction method," *Journal of Magnetism and Magnetic Materials,* 547 (2022) 168958.

[24] B. Aslibeiki, P. Kameli, M. Ehsani, H. Salamati, G. Muscas, E. Agostinelli, V. Foglietti, S. Casciardi, and D. Peddis, "Solvothermal synthesis of MnFe2O4 nanoparticles: the role of polymer coating on morphology and magnetic properties," *Journal of Magnetism and Magnetic Materials,* 399 (2016) 236-244.

[25] http://abulafia.mt.ic.ac.uk/shannon/ptable.php.

[26] B. Aslibeiki, P. Kameli, and M. Ehsani, "MnFe2O4 bulk, nanoparticles and film: A comparative study of structural and magnetic properties," *Ceramics International,* 42 (2016) 12789-12795.